Journal of Maps

ISSN: 1744-5647 (Online) Journal homepage: www.tandfonline.com/journals/tjom20

The geology of the Aracruz pluton (Espírito Santo, Brazil), a Cambrian post-orogenic intrusion in the aftermath of Gondwana amalgamation

Andrea Galli, Max W. Schmidt, Valdecir de Assis Janasi, Felix Soormann, Clara Talca Onken, Alexandra Aregger, Tobias Hendrickx, Samuel Huber, Zoe Kok, Emanuel Pestalozzi, Tabea Stäheli, Luka Wanner & Vinicius Louro

To cite this article: Andrea Galli, Max W. Schmidt, Valdecir de Assis Janasi, Felix Soormann, Clara Talca Onken, Alexandra Aregger, Tobias Hendrickx, Samuel Huber, Zoe Kok, Emanuel Pestalozzi, Tabea Stäheli, Luka Wanner & Vinicius Louro (2024) The geology of the Aracruz pluton (Espírito Santo, Brazil), a Cambrian post-orogenic intrusion in the aftermath of Gondwana amalgamation, Journal of Maps, 20:1, 2411818, DOI: 10.1080/17445647.2024.2411818

To link to this article: https://doi.org/10.1080/17445647.2024.2411818

JOURNAL OF MAPS
2024, VOL. 20, NO. 1, 2411818
https://doi.org/10.1080/17445647.2024.2411818

SCIENCE

OPEN ACCESS Check for updates

The geology of the Aracruz pluton (Espírito Santo, Brazil), a Cambrian post-orogenic intrusion in the aftermath of Gondwana amalgamation

Andrea Galli[a], Max W. Schmidt[a], Valdecir de Assis Janasi[b], Felix Soormann[a], Clara Talca Onken[a], Alexandra Aregger[a], Tobias Hendrickx[a], Samuel Huber[a], Zoe Kok[a], Emanuel Pestalozzi[a], Tabea Stäheli[a], Luka Wanner[a] and Vinicius Louro[b]

[a]Department of Earth Sciences, ETH, Zürich, Switzerland; [b]Instituto de Geociências, Universidade de São Paulo, São Paulo, Brazil

ABSTRACT

We present the first geological map of the Aracruz pluton (Espírito Santo, Brazil), which belongs to the late Cambrian post-orogenic suite that intruded the Nova Venécia metapelites and Ediacaran syn-orogenic S-type granites of the Araçuaí belt. Our mapping coupled with airbone magnetic and radiometric observations reveals that the pluton is not regularly zoned. It is composed of porphyric alkali feldspar granites, into which charnockite and quartz-diorite bands intruded as several pulses while the granites were a deforming crystal mush, and an undeformed central norite emplaced when most movement of the host magma had ceased. Steep-dipping concentric magmatic foliation, magmatic foliation parallel to tectonic foliation in the country rock, the noritic core, and the irregular charnockite and quartz-diorite band alignment suggest buoyancy-driven diapirism as emplacement mechanism. The Aracruz pluton is a superb example of mantle-derived post-orogenic intrusion attesting for the production of continental crust during the final stages of a Wylson cycle.

ARTICLE HISTORY
Received 23 April 2024
Revised 20 September 2024
Accepted 26 September 2024

KEYWORDS
Geological map; aracruz pluton; araçuaí belt; Post-collisional magmatism

1. Introduction

The understanding of post-orogenic magmatism is crucial to unravel the mechanisms governing the growth and/or reworking of the continental crust during the late stages of a Wilson cycle (Bonin, 2004; see review in Goméz-Frutos et al., 2023). In eastern Brazil, the Araçuaí belt and its post-orogenic intrusives mark the end of a Neoproterozoic to Cambrian evolution including the opening and subduction of the Adamastor ocean, the construction of the Rio Doce calc-alkaline magmatic arc and finally the formation of the Araçuaí orogen followed by intense magmatism during orogenic collapse and lithospheric thinning (e.g. Bley de Britos Neves et al., 2014). The Aracruz pluton investigated here is one of about 50 post-orogenic intrusions (see map of the state of Espírito Santo by Vieira et al., 2018; also review in De Campos et al., 2016), more importantly, it is one of the ten larger plutons that display a mafic portion, characteristically noritic to gabbronoritic in composition, and expose an entire magmatic series ranging from norites to granites. It is hence well suited to decipher the magmatic evolution of these plutons, and inform on the magma source, the noritic portion testifying for at least in part a mantle origin. Major questions around these post-orogenic intrusives concern the degree and type of metasomatism in the mantellic source of magma, as well as the interplay between melt evolution by pure crystal fractionation in a closed-system vs. crustal assimilation during magma ascent and emplacement, which requires an understanding of each magma pulse and intrusive rock type. To enable such work, we have undertaken a detailed mapping of the Aracruz pluton, clarifying field relations, relative magma proportions and intrusive successions, and internal structure, which bears on the emplacement mechanism.

2. Geological background

About 700 Ma ago, the Adamastor ocean between the Congo and São Francisco (Brazil) cratons began to close, initiating the final phase of the Wilson cycle in this region and contributing to the amalgamation of the Gondwana continent (Figure 1a and b, Cavalcante et al., 2019; Neves & Cordani, 1991; Pedrosa-Soares et al., 2001; Trompette, 1997). Convergence caused the eastward dipping subduction of the Adamastor ocean below the Congo craton and related mantle-derived calc-alkaline magmatism, with the formation of both the Rio Doce magmatic arc (the G1 suite of De Campos et al., 2004) dated between 630 and 580

CONTACT Andrea Galli andrea.galli@erdw.ethz.ch Department of Earth Sciences, ETH, 8092 Zürich, Switzerland
Supplemental data for this article can be accessed online at https://doi.org/10.1080/17445647.2024.2411818.

Ma (Figueiredo & Campos Neto, 1993; Gonçalves et al., 2016) and the back-arc basin between arc and Congo craton. The subsequent closure of the ocean led to the collision of the two cratons at around 580 Ma, resulting in high-grade metamorphism and intense deformation of the arc intrusives and the dominantly metapelitic back-arc basin sediments of the Nova Venécia complex (Gradim et al., 2014; Vauchez et al., 2007). These two units now form the largest part of the high-grade basement of the Araçuaí orogen, the G1 suite calc-alkaline gneisses located prevalently to the west, and migmatitic metapelites mostly exposed to the east (Figure 1c). The metamorphic grade in the lower crust of the orogen reached temperatures of 750–850 oC at pressures of 5.5-7.5 kbar (Richter et al., 2016), overstepping the muscovite-out and leading to extensive crustal anatexis (Gradim et al., 2014; Sluitner & Weber-Diefenbach, 1989). Three series of crustally derived peraluminous, S-type granitoids are distinguished as G2 to G4 intrusive suites. The volumetrically dominant G2 suite formed 1–20 km large coarse-grained peraluminous intrusions (Figure 1c) characterized by garnet ± cordierite ± sillimanite (Nalini et al., 2000), and mined for ornamental stones in more than a hundred quarries. These peraluminous granites are generally deformed as they crystallized during the early orogenesis (580-545 Ma). Their emplacement was followed by the G3 suite (545-530 Ma), occurring as typically 1–20 m large, less deformed garnet-cordierite-bearing stocks and leucosomes produced by the remelting of both G2 granitoids and metasedimentary rocks during decompression (Alkmim et al., 2006), and by the G4 suite (530-500 Ma), characterized by a few km-sized post-deformational garnet-cordierite-bearing, peraluminous plutons (Pedrosa-Soares et al., 2011). G4 plutons are mined in the state of Minas Gerais for their tourmaline and gems-bearing pegmatitic roof zones exhibiting meter-large crystals, these are not exposed in the state of Espírito Santo.

When convergence halted in the aftermath of the orogenesis, the Araçuaí belt underwent a post-orogenic lithospheric extensional phase, likely as a consequence of gravitational collapse after slab breakoff (Wiedemann et al., 2002). The resulting minor upwelling in the mantle was sufficient to reactivate small-scale metasomatic lithospheric mantle domains and form small melt quantities therein. Likely, this metasomatism stems at least in part from previous arc magmatism, and both extension and the extent of metasomatism were heterogeneously distributed. The mantle-derived, slightly alkaline melts then built the completely undeformed G5 suite (Figure 1c), to which the Aracruz pluton belongs. Through the Araçuaí belt, this post-orogenic magmatism started at ca. 530 Ma, peaked at 500 Ma and lasted to 480 Ma (De Campos et al., 2004, 2016 and references therein). No major geological high-temperature events occurred after the intrusion of G5. The orogen was eroded, the consequent uplift leading to an exposure level that corresponds to 20–25 km depth. Then, in the Miocene, siliciclastic sediments of the Barreiras formation were deposited on the easternmost part of the belt, also just adjacent to the Aracruz pluton (Vieira et al., 1994).

Magmatism of the post-orogenic G5 series is expressed in composite, inversly-zoned plutons (see review in De Campos et al., 2016), but only a few display the full sequence of slightly alkaline norites/gabbronorites to diorites to charnockites to extensive volumes of granites. Furthermore, some plutons also evolve to syenites (intrusions of Venda Nova, Mimoso do Sul, Conceição de Muqui). Noritic to gabbronoritic cores in composite plutons are more abundant in the southern Araçuaí belt (e.g. Mimoso do Sul, Venda Nova, Verza Alegre, Aracruz), yet, larger masses of mafics occur as isolated norite to gabbronorite bodies (Figure 1c, e.g. Conceição de Castello or the 523 Ma São Gabriel de Baunilha norite, Wisniowski et al., 2021, one of the largest producers of 'black granites' worldwide), also predominantly in the south. Norites to gabbronorites and also diorites are absent in the northern half of the G5 intrusive belt, where intrusions are dominated by granites and charnockites (Pedrosa-Soares et al., 2011) and exposure levels are 3–6 km shallower than in the south. In general, the post-orogenic G5 plutons show abundant magmatic but no post-magmatic deformation. The fractionation series maintains orthopyroxene to almost granitic compositions, testifying for relatively dry magma lineages that may or may not have experienced significant crustal contamination (Onken et al., 2024).

In the context of a larger project on the magmatic origin and evolution of the ca. 500 Ma old post-orogenic G5 magmatism in the Araçuaí belt, we mapped the ca. 100 km^2 large Aracruz pluton, which was suspected to have one of the largest noritic cores. In this pluton, the magmatic suites and intrusive relations are excellently preserved and relief is largely sufficient for abundant and good outcrops, although the subtropical weathering takes its toll. Overall, mapping, thin section and geochemical analysis, both for minerals and bulk rocks are well feasible. The only previous maps were the 1:100'000 scale map of the Aracruz area (Fortes et al., 2014) and the excellent 1:400'000 scale 'Mapa Geológico do Estado do Espírito Santo' (Vieira et al., 2018, roughly 400 × 250 km, see a simplified version in Figure 1c), both accomplished by the Geological Survey of Brazil.

3. Methodology

An area of approximately 17 × 13 km comprised between the localities of Ibiraçu, Aracruz, Corrego

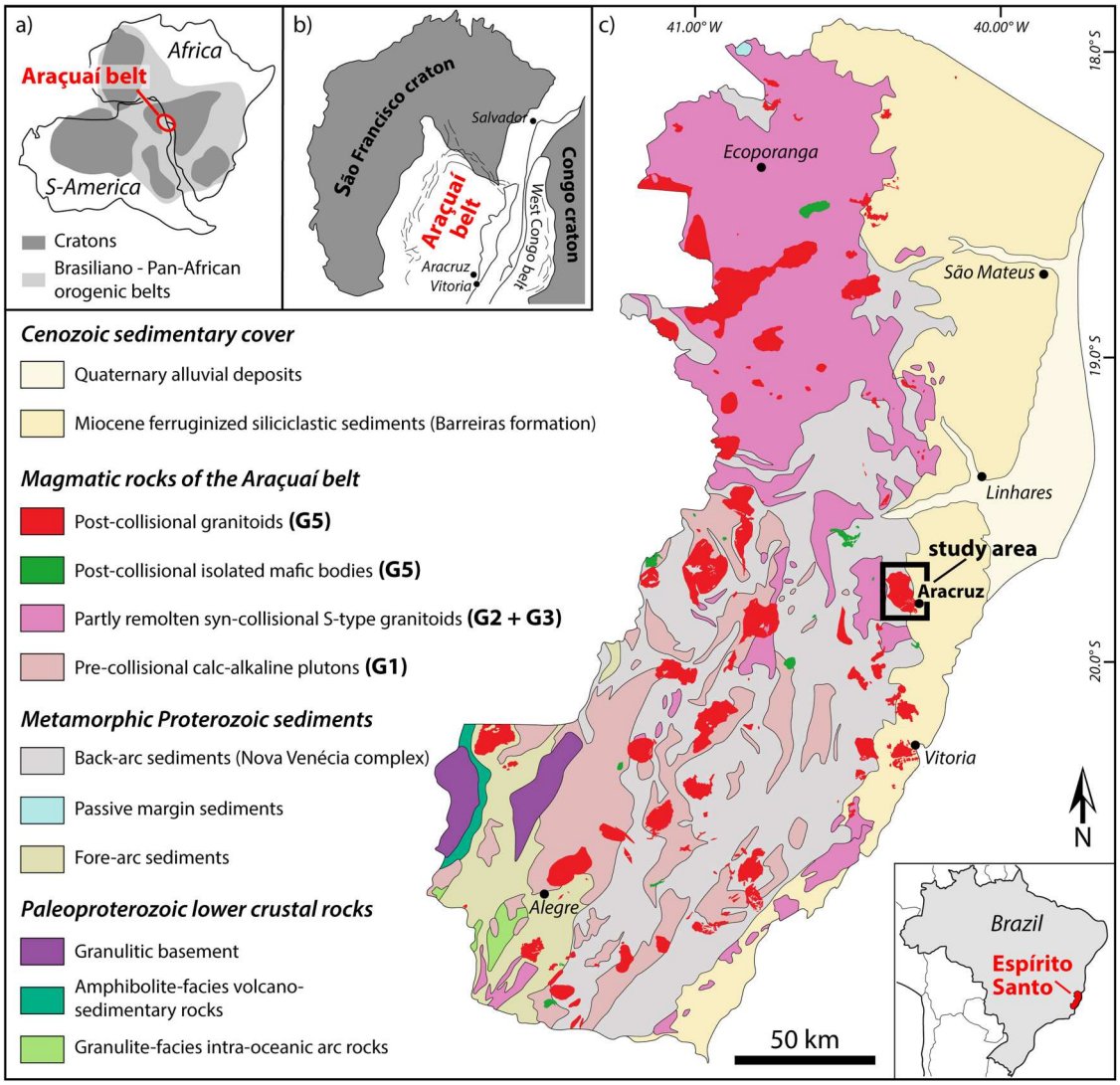

Figure 1. (a) and (b) Location of the Araçuaí belt during the amalgamation of Gondwana; (c) Geological map of the Espírito Santo, modified after Vieira et al. (2018), Inset: study area.

de Agua, Cristal and João Neiva (Figure 2) has been mapped in July 2022 and July 2023 at the 1:10'000 scale and presented here at the 1:50'000 scale (supplementary material). Field mapping has been performed on topographic maps available online by Geobase (Sistema integrado de bases geospaciais do Estado do Espírto Santo, https://geobases.es.gov.br/). Map projection and Coordinate Reference System (CRS) were the UTM 24 S and WGS 84, respectively. Field notes, structural measurements (1028 magmatic foliations in the pluton, 129 dike orientations, 3 quartz vein orientations, 84 main foliations in the country rock, and 2 brittle faults, see supplementary material) and field pictures have been acquired with GPS-integrated Android tablets using the software FieldMOVE (Midland Valley Inc.; Muir, 2015). The location accuracy was typically 3–4 meters. In addition, the magnetic susceptibility of the different rock types has been measured directly in the field. Magnetic susceptibility values were obtained with a portable susceptibility meter model Exploranium Kappameter KT-9 in 'pin' mode. The reported values (Table 1) correspond to the average of 10 measurements on smooth, fresh rock surfaces.

A total of 102 representative fresh rock samples (sample location in supplementary material) comprising all mapped lithologies have been collected and investigated in thin section for their mineralogy, textures and structures using a Nikon Eclipse E400 optical polarizing microscope. Thin section microphotographs have been acquired using a Keyence VHX-6000 digital microscope. For each rock type, a series of 37 microphotographs of representative thin sections have been acquired under both plane and crossed polarized light varying the stage orientation each 10 degrees. A self-made software was then used to produce circular.gif files simulating the view under a petrological microscope. Thin section.gif animations are provided in supplementary material.

Field and petrological observations have been combined with the interpretation of airborne-collected magnetic and gamma-ray spectrometry data. The

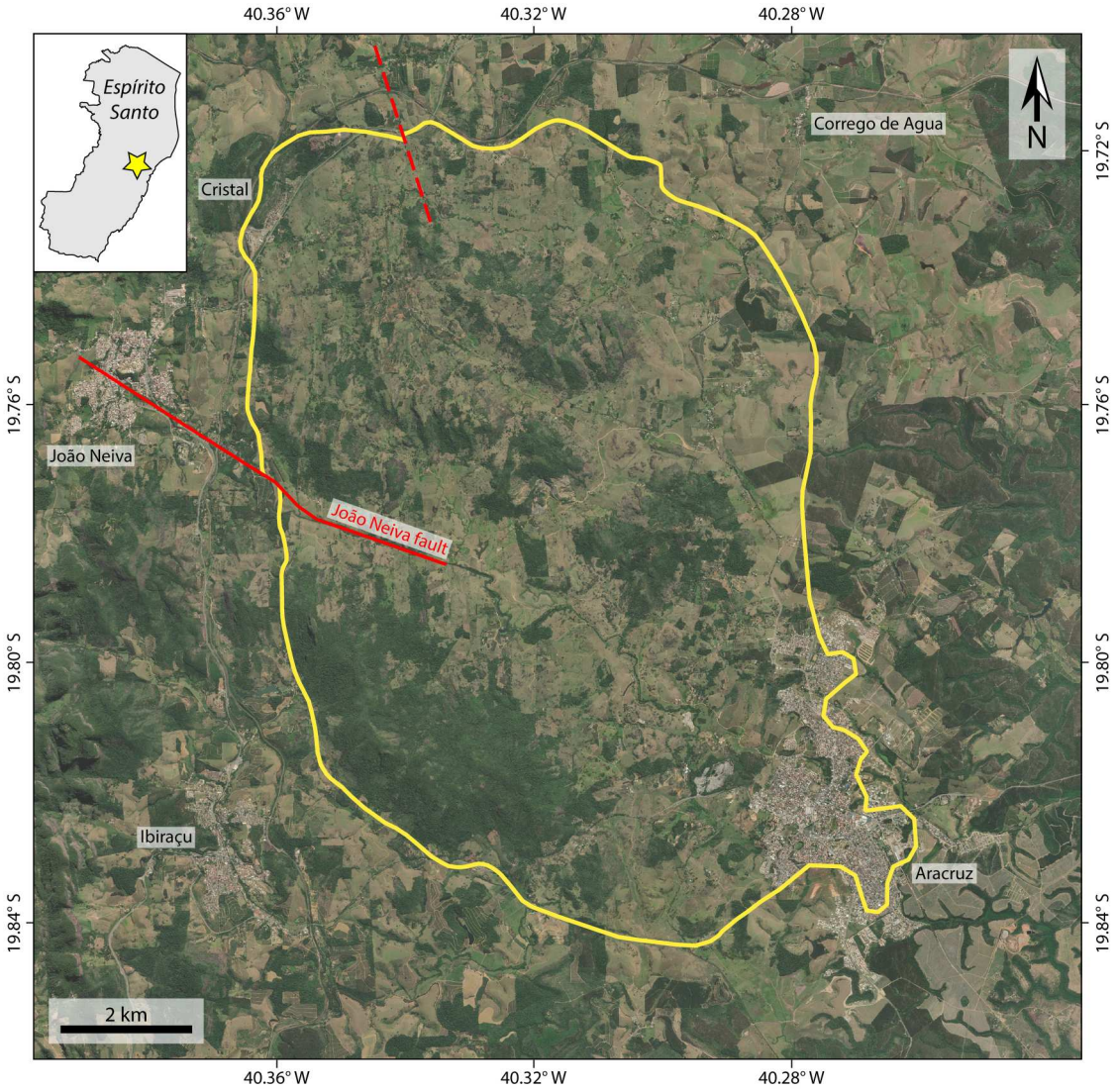

Figure 2. Satellite image of the Aracruz region showing the pluton margin (in yellow) and the location of the João Neiva fault (solid red line) and the only other major brittle structure in the north (dashed red line). Except of the steep dome mountains in the SW (SW of wooded area), the entire pluton is readily accessible with abundant outcrops.

surveys were organized by the Brazilian Geological Service (SGB/CPRM) and performed by Prospectors Aerolevantamentos e Sistemas Ltda between September 2009 and January 2010. The company used Geometrics G-822A Cesium magnetometers, with absolute accuracy better than 3 nT and sensitivity of 0.003 nT at 0.1 s sample rate for the magnetic field. The gamma-ray spectrometers used were the Radiation Solutions RS-500 model of 1024 spectral channel. The flight lines were spaced by 500 m and the tie-lines by 10'000 m, all keeping a 100 ± 15 m terrain clearance in an average speed of 270 km/h (magnetic measures at ca 8 m and gamma-rays at ca 80 m). Both magnetic field and radiometric emission data was pre-processed by the contracted company. After made available at the SGB's GeoSGB platform (https://geosgb.sgb.gov.br/), the magnetic field data was windowed to the target area and filtered to highlight physical contrasts between lithologies and structures. The magnetic anomaly was filtered using a Reduction to the Magnetic Pole (MacLeod et al., 1993) to assess the presence of significant remanent magnetization. We assessed the full extent and boundaries among units within the Aracruz pluton using the Total Horizontal Gradient (THG) on magnetic field data; the magnetic lineaments associated with discontinuities and foliation were outlined using a combination of the THG with the shading of the Tilt Derivative (Miller & Singh, 1994). The Tilt-Derivative shading was obtained by illuminating the filtering product at the azimuth directions 0°, 45°, 90° and 315°. The gamma-ray counts were directly used in a ternary map and evaluated in parallel with the geomorphology given by SRTM data.

4. Results

4.1. Geographic situation and topography

The Aracruz pluton forms a well-rounded 15 × 9 km ellipsoid, the long axis tending NNW-SSE (Figure 2).

Table 1. Description of the mapped lithological units.

Rock unit	Surface (Km^2)	% of pluton area	Major minerals	Accessories	Texture	Structure	Magnetic susceptibility (x10e-3 SI)
Aracruz pluton							
Norite	0.88	0.9	Opx, Cpx, amphibole, biotite, plagioclase, quartz, alkali feldspar, opaques	Apatite, zircon	Holocrystalline, equigranular, mid- to coarse-grained	Massive	28.0 – 66.2 Average: 43.3
Charnockite	22.47	21.9	Opx, amphibole, biotite, plagioclase, quartz, alkali feldspar, opaques	Sphene, apatite, zircon, chlorite, secondary muscovite	Holocrystalline, equigranular, mid- to coarse-grained	Massive	20.3 – 77.4 Average: 49.3
Quartz-diorite	6.00	5.8	Amphibole, biotite, plagioclase, quartz, alkali feldspar, opaques + rare Opx	Zircon, apatite	Holocrystalline, equigranular, fine- to mid-grained	Foliated	2.9 – 66.0 Average: 45.1
Homogeneous porphyric grey alkali feldspar granite	45.60	44.4	Biotite, quartz, plagioclase, alkali feldspar, opaques ± amphibole	Chlorite, apatite, zircon, secondary muscovite	Holocrystalline, mostly porphyric, only in the southeasternmost part equigranular, coarse-grained	Mostly foliated	0.46 – 37.4 Average: 15.1
Heterogeneous porphyric grey alkali feldspar granite	27.55	26.8	Biotite, quartz, plagioclase, alkali feldspar, opaques, locally amphibole	Chlorite, apatite, zircon, secondary muscovite	Holocrystalline, mostly porphyric, only in the southeasternmost part equigranular, coarse-grained	Mostly foliated	Not measured
Porphyric pink alkali feldspar granite	0.23	0.2	Biotite, quartz, plagioclase, alkali feldspar, opaques	Chlorite, apatite, zircon, secondary muscovite	Holocrystalline, mostly porphyric, only in the southeasternmost part equigranular, coarse-grained	Mostly foliated	9.6
Pegmatite and aplite dikes	-	-	Biotite, quartz, plagioclase, alkali feldspar	Apatite, opaques, zircon	Holocrystalline, equigranular, coarse-grained	Massive	4.7
Gabbronoritic and other mafic to intermediate dikes	-	-	Opx, Cpx, biotite, apatite plagioclase, quartz, alkali feldspar, opaques ± amphibole	Zircon	Holocrystalline, equigranular, fine- to mid-grained	Massive	19.2 – 57.2 Average: 35.9
Nova Venécia complex							
Metapelitic series	-	-	Biotite, garnet, quartz, plagioclase, alkali feldspar ± cordierite, sillimanite	Apatite, zircon, secondary muscovite	Equigranular, granoblastic leucosomes and lepidoblastic-neatoblastic melanosomes, mid- to coarse-grained	Foliated	0.14 – 0.17
S-type granite	-	-	Biotite, garnet, plagioclase, quartz, alkali feldspar	Apatite, zircon , opaques	Holocrystalline, equigranular, mid- to coarse-grained	Foliated	0.52
Banded orthogneiss	-	-	Biotite, quartz, plagioclase, alkali feldspar	Apatite, zircon	Equigranular, granoblastic-lepidoblastic, mid- to coarse-grained	Foliated	Not measured
Mesozoic fine-grained basaltic dike	-	-	Plagioclase, cpx, iddingsite, opaques		Holocrystalline, equigranular, fine- to mid-grained, ophitic	Massive	Not measured
Cenozoic sediments							
Ferruginized sandstone	-	-	Quartz, goethite, hematite,		Mid- to coarse-grained	Massive	Not measured

The town of Aracruz covers its SE corner, the western border is close and parallel to the N-S interstate highway (BR101) connecting Rio de Janeiro to Natal, with the town of João Neiva just W of the pluton and W of the pluton's center. Agriculture is a combination of cattle, coffee plantations and occasional other fruits. All roads are dirt roads, but grant good access to the pluton except of the three steep mountain chains.

The southern, western and central parts are made up by three major mountain chains with 200–700 m relief, striking roughly E-W, and building about 60% of the pluton. Their larger part and also most summits are constituted by a quite homogeneous porphyric grey alkali feldspar granite (see below), which is clearly the lithology most resistant to weathering. The northern and eastern margins instead end in slightly hilly flatlands, with quite sparse outcrops towards the intrusion's borders. The eastern rim (north of the city of Aracruz) is topographically flat and submerges in part under Cenozoic sediments, which continue to the Atlantic coast (Figure 1c). The sediments are weathered to soils (not mapped), but in three hillsides areas of 50–300 m extension exhibit typically 10–30 cm large, massive, yet porous nodules. These are composed of a hematite-goethite-cemented immature quartz-dominated sandstone, are ubiquitous on the ground and likely belong to the 26–20 Ma old Barreiras formation (Monteiro et al., 2022). Biologically driven weathering reactions induced the mineralization of some irregular layers within this formation, which then form the quite hard concretions now exposed through weathering. (U-Th)/He ages of authigenic hematite and goethite cement yielded ages between 5 and 0.6 Ma (Monteiro et al., 2022). Nevertheless, occasionally, basement outcrops of the Nova Venécia metapelitic series or banded orthogneisses can be found in the east of the Aracruz pluton, such that its limit may be delineated quite precisely.

Two major brittle faults cut into the Aracruz pluton (already mapped on the 1:400'000 scale map of the Espírito Santo, Vieira et al., 2018). One is well visible in satellite images, strikes WNW-ESE, forming a 30 km long valley that runs from the WNW into the town of João Neiva, where the fault bends towards the east, forming a surprisingly straight 7 km long E-W valley in the Aracruz pluton (Figure 2). The 'João Neiva fault' causes a mappable displacement of about 300 m at the plutons border and an increasingly lesser displacement of magmatic bands progressing to the east before dying off near the plutons centre. The second larger fault cuts from the NNW into the northwestern margin of the pluton, but no clear topographical nor geological evidence was found, almost no displacement is observable on map view, the flat topography and occasional outcrops not allowing any detailed investigation.

4.2. Major mappable lithological units

All together six mappable intrusive lithologies and two dike types were defined for the Aracruz pluton, addended by the Mesozoic fine-grained basaltic dike, the country rocks of the Nova Venécia complex and the Tertiary sediments. Lithological contacts within the pluton and contacts between intrusives and country rocks are generally poorly exposed. In the following, mapped lithologies are described for their field occurrence and mineralogy as observed in thin section. The most relevant features, including their areas, are summarized in Table 1.

4.2.1. Cambrian, post-orogenic rocks of the aracruz pluton

4.2.1.1. Norite. The norite forms one larger homogenous body of 1.5 km x 700 m in the central part of the pluton heavily mined for ornamental stones (Figure 3a), as well as several smaller bodies typically 50–200 m large dispersed across the pluton and across all lithologies. The norite is homogeneous, holocrystalline, equigranular, mid- to coarse-grained with 0.5-1 cm grain sizes of dominantly orthopyroxene (opx), plagioclase and biotite, a few percent of clinopyroxene (cpx), opaques and apatite, and some minor amphibole, interstitial quartz and alkali feldspar. The structure is massive and does not show flow features (Figure 3b and c). There are a few porphyric alkali feldspar granite dikes well visible in the walls of the two quarries, the larger dikes (0.5-1 m thick) occur every few hundred meters. Furthermore, about one out of 20 quarried blocks (2.5 × 2.5 × 5 m sized) would show minor, mostly straight leucocratic dikelets (Figure 3b and c). Texturally, these intruded in a late magmatic stage, still forming diffusive phlogopite-rich rims according to alkali feldspar^{granite} + opx^{norite} = phlogopite (Figure 3b). More fine-grained rounded mafic enclaves, swarm of enclaves and gabbronorite dikes are rare (Figure 3c and d). In thin section (Figure 4a and supplementary material), the norite is composed of subhedral, equant, 0.5–5 mm large, slightly pinkish opx (15-25 vol-%) and slightly greenish cpx (<5 vol-%), both locally in part replaced by green amphibole (<5 vol-%), euhedral, tabular, up to 2 mm in size plagioclase (40-50 vol-%), subhedral to euhedral, 0.5–4 mm large, unoriented biotite flakes (15-30 vol-%), anhedral, up to 1 mm large opaques (5-10 vol-%) often included in or adjacent to biotite and opx, subhedral to euhedral, prismatic, up to 1 mm large apatite grains, and anhedral, up to 1 mm large and interstitial quartz (<5 vol-%) and alkali feldspar (<5 vol-%). Zircon is accessory.

4.2.1.2. Charnockite. The charnockite occurs as 2 × 12 km large, elongated bodies and tens of smaller bodies across the whole pluton. It is generally holocrystalline,

Figure 3. Field aspect of norite, charnockite, quartz-diorite and homogeneous porphyric grey alkali feldspar granite: (a) rock cut exposure of the western norite quarry (040°19′05.020591″W, 19°46′21.990933″S); (b) leucocratic dike in the massive norite displaying not completely sharp and straight contacts to the host norite and diffusive phlogopite-rich selvedges; (c) isolated rounded, fine-grained mafic enclave in massive norite; (d) centimetric thick leucocratic dike and swarms of mafic enclaves in massive norite (040°19′02.320620″W, 19°46′20.966532″S). All of these features are quite rare, the equigranular norite is characterized by its homogeneity; (e) mid- to coarse-grained, massive charnockite with rare leucocratic dikes (040°19′33.136076″W, 19°45′26.115117″S); (f) slightly foliated, fine-grained quartz-diorite characterized by the occurrence of a network of leucocratic dikes (040° 19′31.509160″W, 19°45′14.384563″S); (g) homogeneous porphyric grey alkali feldspar granite characterized by the preferred orientation of centimetric alkali feldspar crystals and leucocratic layers, both defining a penetrative magmatic foliation (040° 20′31.127915″W, 19°45′32.408422″S); (h) oriented alkali feldspar crystals in the homogeneous porphyric grey alkali feldspar granite (040°20′31.127915″W, 19°45′32.408422″S).

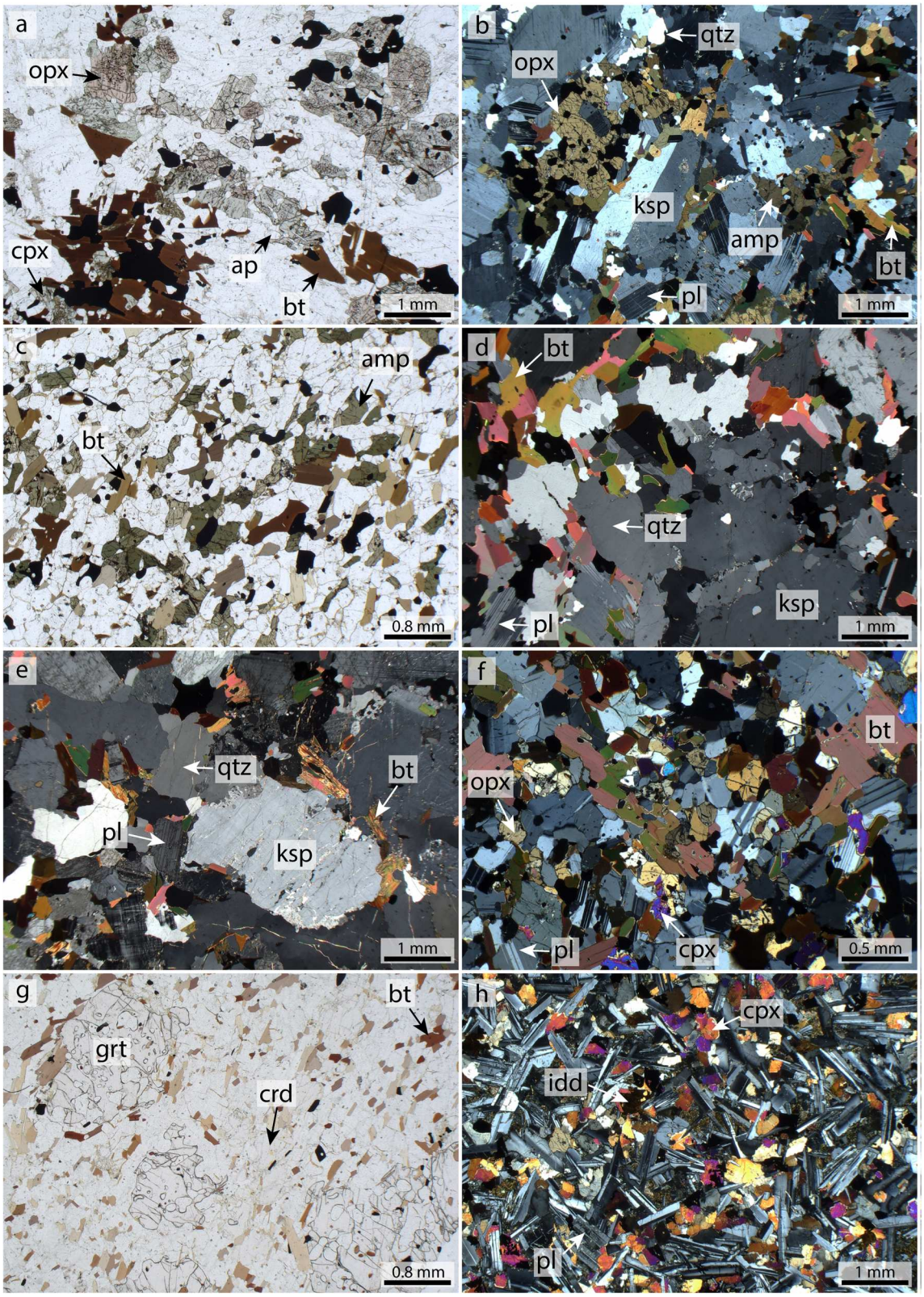

Figure 4. Photomicrographs of principal rock types: (a) pinkish orthopyroxene and brownish biotite in norite (plane polarized light, sample AR22-10); (b) opx surrounded by amphibole and biotite in charnockite (cross polarized light, sample AR22-63); (c) slightly oriented greenish amphibole and biotite grains in quartz-diorite (plane polarized light, sample AR22-91); (d) homogeneous porphyric grey alkali feldspar granite mostly constituted of quartz, plagioclase, alkali feldspar and biotite (cross polarized light, sample AR22-40); (e) alkali feldspar-rich, biotite-poor porphyric pink alkali feldspar granite (cross polarized light, sample AR22-58); (f) opx and cpx together with biotite and plagioclase are the main mineral phases in gabbronorite dikes (cross polarized light, sample AR22-20); (g) garnet-cordierite-bearing, biotite-rich melanosome in the upper amphibolite facies Nova Venécia metapelites (plane polarized light, sample AR22-80); (h) ophitic texture defined by tabular plagioclase, cpx and iddingsite in fine-grained basaltic dike of probably Late Cretaceous age.

mid to coarse-grained, equigranular and massive, lacking any penetrative magmatic foliation (Figure 3e). Mafic minerals are opx, amphibole and biotite. Locally, the charnockite is cut by mostly coarse-grained to pegmatitic dikes of porphyric granite, a preferred orientation is only visible in 1/3 of the outcrops. These dikes have diffuse boundaries, sometimes dissolve into the charnockite and have irregular patterns, all testifying for being injected during partial solidification of the host charnockite. Sometimes, these dikes form a network leading to characteristic outcrop patterns. A continuum in lithotype exists between the charnockite and the quartz-diorite, hence the dominant features were chosen to identify the map unit, a difficult choice in about 10% of the outcrops. While mapping, we used the massive granularity, the larger grain size and the often well visible quartz and alkali feldspar for charnockite, and the finer-grained grain size and the occurrence of acicular amphiboles to characterize a quartz-diorite. In thin section (Figure 4b and supplementary material), opx (5-10 vol-%) occurs as subhedral, up to 2 mm large, equant grain, often surrounded by green amphibole and opaques, amphibole (15-20 vol-%) forms subhedral, up to 3 mm large, prismatic greenish grains often rimming or replacing opx, biotite (15-20 vol-%) is subhedral to euhedral, up to 3 mm large and micaceous, opaques (<5 vol-%) are anhedral, up to 0.1 mm large and often in contact with opx. Plagioclase (40-45 vol-%), quartz (10-15 vol-%) and alkali feldspar (5-10 vol-%) are anhedral to subhedral, 0.5-2 mm large and equant. Sphene, apatite, zircon, chlorite and secondary muscovite are accessories.

4.2.1.3. Quartz-diorite. The quartz-diorite constitutes three major, up to 1 × 10 km large, elongated bodies between João Neiva and Aracruz, and many smaller mappable bodies within the porphyric alkali feldspar granite. The quartz-diorite is the most finely grained major lithology, is holocrystalline, equigranular and typically shows a penetrative magmatic foliation defined by planarly oriented mm-sized acicular amphibole and biotite platelets, a lineation is not observed. The felsic mineral is mostly plagioclase, quartz is rarely visible by hand lens. Typically, there are series of 1–10 cm thin granitic dikes with decimeter to meter inter-dike spacings completely parallelized into the magmatic foliation and also networks of conjugate granite dikes with a symmetry plane at a large angle to the magmatic layering (Figure 3f). In thin section (Figure 4c and supplementary material), the quartz-diorites is composed of subhedral to euhedral, 0.2–2 mm large, columnar, greenish amphibole (10-20 vol-%), which typically display numerous apatite inclusions, subhedral, up to 2 mm large, micaceous biotite (15-25 vol-%), anhedral, up to 0.5 mm large opaques (<5 vol-%), and subhedral to euhedral, up to 1 mm large plagioclase (40-50 vol-%), quartz (10-15 vol-%) and alkali feldspar (5-10 vol-%) grains. Zircon and apatite are accessories. Locally, in the quartz and alkali feldspar poor domains, subhedral, up to 1 mm sized, equant opx occur, often partly replaced by green amphibole.

4.2.1.4. Homogeneous porphyric grey alkali feldspar granite. The homogeneous porphyric grey alkali feldspar granite is the main intrusive of the Aracruz pluton and dominates the central and southern parts of the intrusion. This granite is holocrystalline, coarse-grained, porphyric and characterized by texturally dominant, 2–5 cm large alkali feldspar crystals mostly well aligned in magmatic foliation planes (Figure 3g and h). Characteristically, outcrops are >99% granite, with few other features such as isolated enclave and swarms of enclaves that can be followed over tens of meters. Most characteristic is the uniform texture and long sections of almost entirely homogeneous granite. Exclusively near the southeastern border of the intrusion, this granite becomes equigranular, lacking the porphyric alkali feldspar, at the same time, it presents more heterogeneities, such as mafic enclaves and swarm of enclaves. All other features are similar to the homogeneous porphyric alkali feldspar granite. In thin section (Figure 4d and supplementary material), the porphyric alkali feldspar granite is mostly composed of euhedral, up to 5 cm large, prismatic, often twinned alkali feldspar (30-35 vol-%), subhedral, 1–2 mm large, equant quartz (30-35 vol-%) and plagioclase (15-20 vol-%), subhedral to euhedral, up to 3 mm large biotite flakes (10-20 vol-%), which occasionally are slightly chloritized, and subhedral, up to 0.3 mm large opaques (<5 vol-%). Chlorite, apatite, zircon and secondary muscovite are accessories. Locally, subhedral, up to 2 mm large, short prismatic amphibole (<5 vol-%) grains occur.

4.2.1.5. Heterogeneous porphyric grey alkali feldspar granite. The northern part of the Aracruz pluton is dominated by a similar porphyric granite, but this granite is fairly heterogeneous at an outcrop scale, with 5-20% being constituted by heterogeneities. Typically, this granite is characterized by well aligned, rounded or angular lengthy mafic enclaves that likely constitute disrupted mafic dikes, by up to 20 m long segments of mafic dikes, characteristically 10–100 cm across, by numerous 'schlieren' of mafic minerals, and by a much larger number of pegmatitic dikes than in the homogeneous porphyric granite (Figure 5a–c). In thin section, there is no difference to the homogeneous granite.

4.2.1.6. Porphyric pink alkali feldspar granite. Four mappable pink granites 150–700 m in size were found in the central and eastern part of the intrusion,

Figure 5. Field aspect of heterogeneous porphyric grey alkali feldspar granites, porphyric pink alkali feldspar granite and country rocks: (a) decimetric to metric swarm of fine-grained, rounded mafic enclaves in the heterogeneous porphyric grey alkali feldspar granite (ca. 25 m large boulder); (b) fine-grained mafic dike in the heterogeneous porphyric grey alkali feldspar granite (040° 20′05.407597″W, 19°46′50.546908″S); (c) isolated, fine-grained mafic enclave in the heterogeneous porphyric alkali feldspar grey granite (040°17′52.159670″W, 19°43′49.153125″S); (d) coarse-grained porphyric pink alkali feldspar granite (picture width 18 cm, 040°19′38.879136″W, 19°47′07.860843″S); (e) stromatic texture in migmatitic paragneisses of the Nova Venécia complex, displaying coarse-grained, garnet-bearing leucosomes alternated with more fine-grained garnet-biotite-sillimanite rich melanosomes (040°19′51.985416″W, 19°43′04.425420″S); (f) slightly foliated, coarse-grained, garnet-bearing S-type G2 granite (picture width 25 cm, 040°19′50.065477″W, 19°43′05.315827″S); (g) biotite-rich banded orthogneiss (040°15′30.864923″W, 19° 45′00.661790″S); (h) raft of garnet-rich paragneiss in locally garnet-bearing porphyric grey alkali feldspar granite (040° 18′00.217771″W, 19°45′52.066067″S).

but several other small occurrences were observed in both the charnockites and the porphyric grey alkali feldspar granite. This granite is texturally similar to the homogenous porphyric grey alkali feldspar granite, but the well-oriented alkali feldspar crystals of 2–5 cm size are pink to red in colour (Figure 5d), a consequence of finely dispersed hematite. Likely these granites have undergone some modification by deuteric fluids and served as conduit zones for their rise towards the surface (see below). In thin section (Figure 4e and supplementary material), these granites are only little different from the homogenous porphyric grey alkali feldspar granite. Quartz (35-40 vol-%) and alkali feldspar (35-40 vol-%) are present in slightly higher amount, while plagioclase (10-15 vol-%) and biotite (5-10 vol-%) are slightly less abundant.

4.2.1.7. Pegmatite and aplite dikes. All lithologies have abundant syn-magmatic, coarse-grained, porphyric to pegmatitic dikes which have not been further investigated and are generally too small to be mapped, typically <1 meter in thickness. They are almost always roughly aligned with the magmatic foliation, their borders are never sharp and undulate slightly, both consistent with their emplacement into a fairly solidified still melt-containing and moving crystal mush. Macroscopically, pegmatitic dikes are holocrystalline, equigranular, coarse-grained, massive and contain alkali feldspar, quartz, plagioclase and biotite. Muscovite has never been observed. Note that scapolite from a few not precisely located dikes in the southern mountain chain are described by Bento et al. (2022), which is to our knowledge the only scientific publication specific to the Aracruz pluton. In thin section (supplementary material), pegmatites are composed of euhedral, up to 5 cm, prismatic alkali feldspar (40-45 vol-%) with perthitic exsolution, subhedral to euhedral, up to 5 mm, tabular biotite (5-10 vol-%), and subhedral, 1–3 mm large quartz (40-45 vol-%) and plagioclase (5-10 vol-%). Apatite, opaques and zircon are accessories.

Very few dikes show features characteristic of being intrusive into a completely solidified host rock. The few ones sampled are greenish-grey, fine-grained aplites, that sharply crosscut the magmatic foliation of the host porphyric alkali feldspar granites or occur within charnockites. They are mostly composed of quartz, two feldspars and biotite. In thin section, subhedral, up to 1 mm large quartz (40-45 vol-%) and subhedral, up to 1 mm large alkali feldspar (40-45 vol-%) dominate, plagioclase (5-10 vol-%) occurs as subhedral, up to 0.5 mm large grain, biotite (5-10 vol-%) as subhedral, up to 1 mm large, tabular grains, whereas apatite, zircon and opaques are accessories (supplementary material).

4.2.1.8. Gabbronorite and other mafic to intermediate dikes. The only gabbronorite dikes observed occur in the norite quarry as continuous or partly disrupted dikes (Figure 3d), suggesting that more of these would be present, only that in the field, they are hard to distinguish from other fine-grained mafic and intermediate dikes and enclaves in e.g. the heterogeneous granite. Gabbronorite dikes (Figure 4f and supplementary material) are holocrystalline, fine- to mid-grained, equigranular, massive and mostly composed of subhedral to euhedral, up to 1 mm large, equant opx (10-15 vol-%) and cpx (15-20 vol-%), typically displaying numerous tiny opaque inclusions, subhedral, 0.1-1 mm large biotite flakes (30-35 vol-%), often concentrated around opx, subhedral, up to 0.5 mm large plagioclase (30-35 vol-%), rounded apatite (<5 vol-% vol-%) and abundant anhedral opaques (<5 vol-%) disseminated in the rock matrix or included in both pyroxenes. Quartz (<2 vol-%) and alkali feldspar (<2 vol-%) are present in minor amounts, while zircon is an accessory phase. Other mafic to intermediate dikes lack cpx, generally have amphibole and a larger amount of quartz and alkali feldspar.

4.2.2. Mesozoic fine-grained basaltic dike

One fine-grained basaltic dike has been mapped in the southern part of the pluton. The dike is a few meters thick, 30–40 m long, strikes NW-SE, is massive, dark coloured and displays sharp and straight boundaries to the host porphyric grey alkali feldspar granite. In thin section (Figure 4h and supplementary material), euhedral, up to 1 mm large, tabular plagioclase (55-65 vol%), subhedral 0.2-2 mm large, equant cpx (25-30 vol-%), and brownish, subhedral, up to 0.3 mm large iddingsite (5-10 vol-%) likely replacing olivine define an ophitic texture. Opaques (5-10 vol-%) are present as subhedral to euhedral, up to 0.2 mm large grains. Numerous dikes and swarms of dikes with similar field occurrence, mineralogy and texture are reported from the whole Espírito Santo (e.g. Santiago et al., 2020 and references therein). They intruded during the Lower Cretaceous as result of the west break-up of Gondwana and opening of the Atlantic ocean.

4.2.3. Country rocks

On the map, we did not differentiate between distinct types of country rocks. Around almost the entire intrusion, the country rock is formed by a garnet-sillimanite-rich, sometimes cordierite bearing migmatitic paragneiss (Figure 5e) belonging to the Nova Venécia metapelitic series, and locally, by up to 50 m sized stocks and metric dikes of S-type granite (Figure 5f), which likely represent accumulations of mobilized in-source leucosomes classically attributed to the Ediacaran G2 magmatic suite. The only other country rock is a heavily deformed, equigranular garnet-free, biotite-rich banded orthogneiss in the northeastern corner of the pluton (Figure 5g), well visible on the geomagnetic map (Figure 8). Along the entire outer pluton rim, the country rock shows no apparent

contact metamorphism nor evidences of (re)melting in the immediate vicinity of the pluton contact. Furthermore, a total of ten 50–650 m long lenses and a number of smaller angular to rounded xenoliths of migmatitic paragneiss occur in the Aracruz intrusives (Figure 5h), yet, no systematics with the host magma can be observed. Some of the smaller paragneiss lenses are near the rim and elongated within the rim-parallel flow features. Occasionally, the porphyric grey alkali feldspar granite in the immediate vicinity may contain some garnet, likely a result of chemical assimilation of the peraluminous metapelitic material (Figure 5h).

4.2.3.1. Nova Venécia complex. The migmatitic paragneisses are characterized by the alternation of coarse-grained, granoblastic, centimeter thick in-situ leucosome bands bearing up to 1 cm large garnet ± cordierite and mid-grained, lepidoblastic-nematoblastic bands of biotite-garnet-cordierite ± sillimanite-rich melanosomes (Figure 5e). Leucosomes are generally parallel to the main foliation but locally cut across the fabric testifying for syn-kinematic anatexis. In thin section, leucosomes are mostly constituted of subhedral to euhedral quartz (40-45 vol-%), plagioclase (5-10 vol-%), perthitic alkali feldspar (40-45 vol-%), garnet (5-10 vol-%), biotite (<5 vol-%), and locally cordierite (<5 vol-%). Melanosomes (Figure 4g and supplementary material) are composed of subhedral, up to 4 mm large, equant garnet (10-15 vol-%), abundant aligned, tabular, up to 1 mm large biotite flakes (20-30 vol-%), subhedral quartz (25-30 vol-%), alkali feldspar (5-10 vol-%) and plagioclase grains (20-30 vol-%), subhedral, up to 1 mm large, equant cordierite (5-10 vol-%), which typically displays yellowish pleochroic haloes around zircon inclusions, and locally euhedral, up to 2 mm large, oriented, prismatic sillimanite (<5 vol-%). Apatite, opaques, zircon and secondary muscovite are accessories.

4.2.3.2. S-type granite (G2 suite). The S-type granites are fairly homogeneous, holocrystalline, equigranular, mid- to coarse-grained, slightly foliated and almost always bear garnet (Figure 5f). In thin section (supplementary material), subhedral to euhedral, up to 3 mm large, equant quartz (40-45 vol-%), plagioclase (20-25 vol-%) and alkali feldspar grains (35-40 vol-%) constitute most of the rock. Subhedral, 0.5-2 mm large, slightly oriented biotite flakes (5-10 vol-%) and up to 2 mm large, rounded garnet (5-10 vol-%) are present in minor amount, while apatite, zircon and opaques are accessories. In these granites, muscovite has never been observed, indicating that migmatization conditions exceeded the stability of muscovite.

4.2.3.3. Banded orthogneiss. The banded orthogneiss constitutes about 1 km of pluton contact in the northeast, is mid- to coarse-grained and composed of granoblastic bands of quartz (35-40 vol-%), plagioclase (30-35 vol-%) and alkali feldspar (5-15 vol-%), and lepidoblastic bands of biotite (10-20 vol-%), with apatite and zircon as accessories. Whether this orthogneiss belongs to the Nova Venécia complex or G1 suite is unknown.

4.2.4. Sedimentary cover: ferruginized sandstones

This rock unit occurs occasionally in the eastern part of the pluton, yet mainly on three hillsides (see map). Direct solid outcrops have not been found, the hill sides are swarming with characteristic, well rounded, brown-reddish, cavity-rich boulders, typically one decimeter to half a meter in size, the maximum size observed was metric. Most of these pebbles to boulders are well weathered, and fragment into many grains when hammered. Fresh solid rocks have a red matrix, with white quartz grains and large irregular 0.5-5 cm wide round cavities coated with hematite and goethite. A few exceptionally dense specimens are heavily mineralized, yielding a metallic luster to cm2-large zones in the rock. In thin section (supplementary material), besides hematite and goethite (10-20 vol-%), edgy and often broken quartz grains (30-40 vol-%) are embedded in the matrix. Minerals with light brown colours (10-20 vol-%) were not further determined but are probably oxidized Fe-ore. The walls of the abundant voids (20-30 vol-%) are covered with white to slightly gray-shaded coatings of quartz. This unit belongs to the 26–20 Ma old Barreiras formation (Monteiro et al., 2022).

4.2.5. Secondary features

The most striking about secondary features is the lack thereof. Not a single greenschist facies vein has been found during the intensive mapping, and only very occasional quartz veins occur. Overall, this confirms the fairly dry nature of the magmas constituting the pluton, leaving little deuteric fluid for alterations. Nevertheless in a few places, spectacular sets of 5–10 cm thick, 0.5-3.0 m long tension gaps, were observed. These are filled with idiomorphic quartz, alkali feldspar and biotite packages that clearly grew into fluid filled cracks in the rocks. Along their plane, these pockets are roundish and several square meter in size.

Furthermore, no solid-state shear zones have been observed, the only major fault forms a valley and is covered by quaternary sediments, its existence can only be deduced from the resulting mappable displacement. In general fractures have not led to significant visible displacement, brittle deformation is very minor.

4.3. Geomorphology, weathering and erosion

The subtropical weathering generally leads to a rough black rock surface, making it hard to recognize any

units from the distance or in satellite images, aggravating the mapping effort. Nevertheless, after having mapped the entire pluton, several features stand out: the homogenous porphyric grey alkali feldspar granite builds almost all of the high mountains (Figure 6a), half of them shaped as dome mountains, similar to the world-famous Pão de Açúcar in Rio de Janeiro. At the other extreme, the fine-grained, well-foliated quartz-diorite is the weakest lithology in the landscape, forming depressions on ridges and valleys on mountain sides (Figure 6b). In the flatter parts, quartz-diorite outcrops are level with the grassy landscape.

The heterogeneous porphyric grey alkali feldspar granite is well recognizable through its rough surface, with typically 10 cm deep erosion features reflecting the finer grained portions (Figure 6c). Deeply incised gullies characterize steep surfaces, yet, these occur occasionally also in the homogeneous granite. In the flatter parts of the landscape, heterogeneous granite often forms depressions or flat areas in the grass. Instead, the homogeneous porphyric grey alkali feldspar granite forms characteristically round cupola-shaped hills that stand well out, and exhibits from the distance comparatively smooth surfaces. The charnockites do have little specific surface features.

4.4. Intrusive relations

Structurally, the porphyric alkali feldspar granites are the oldest magma into which all others intruded. Charnockite and quartz-diorite form large, typically hundreds of meters wide, mostly continuous bands in the homogenous granite, while these bands are disrupted in the heterogeneous granite forming widely dispersed, yet flow-aligned swarm of enclaves and more isolated enclaves of typically 0.5-10 m in size (Figure 5a and b). Both the charnockite and quartz-diorite are injected by porphyric grey alkali feldspar granite dikes on a 1–10-meter scale (Figure 3e and f). In the quartz-diorite, a first generation of dikes is perfectly aligned in its flow planes, these intruded during magmatic deformation. The set of conjugated dikes is then consistent with intrusion after the host quartz-diorite has largely crystallized due to its higher melting point or lower interstitial melt fraction

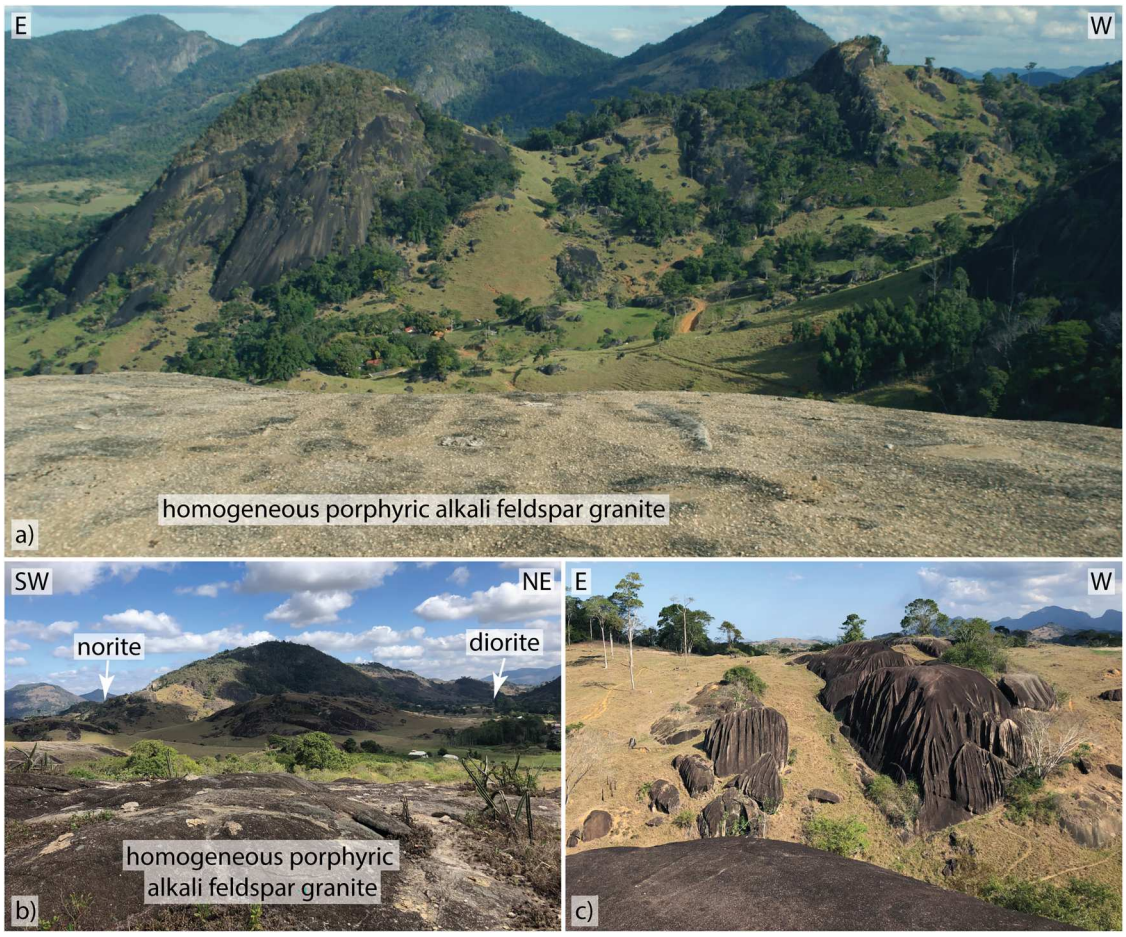

Figure 6. Morphological characteristics of the mapped rocks: (a) the homogeneous porphyric grey alkali feldspar granite typically constitutes the high mountains (view direction towards S, in the background the southwestern dome mountains); (b) fine-grained quartz-diorite are the weakest rock type and build depression and valley in the landscape; (c) erosion forms characteristic for the heterogeneous porphyric grey alkali feldspar granite.

compared to the granite. The charnockite is equally intruded by porphyritic granite, but is massive (Figure 3e), testifying for a transition from a relatively low viscosity mush to an almost solidified rock after injection. Finally, the large noritic body is likely a late-stage intrusion into the lesser solidified, largely granitic centre of the pluton. The norite shows short contacts to a charnockite and quartz-diorite band at its western and eastern margin, respectively, but has no dioritic or charnockitic hull. It is further characterized by its equigranular massive and homogeneous appearance and does not exhibit any flow features, suggesting that deformation stopped as the central part of the pluton was still hot. In addition, the higher solidus temperature of the norite compared to the granite suggests relative rapid crystallization after intrusion. Furthermore, more heterogeneous border facies are in general common to all lithologies (for the norites, the border could not be observed). In particular, also the otherwise homogenous granite become more heterogeneous towards intrusive contacts, altogether testifying for a concomitant semi-liquid state of all magmas.

4.5. Structural geology

In the pluton, 1028 measurements of magmatic foliation (defined by aligned alkali feldspar crystals in the porphyric granites, amphibole ± biotite in the quartz-diorites and rarely also in the charnockites, preferred enclave direction and magmatic layering) and 129 dike orientations of both granitic and more mafic composition have been taken. Furthermore, 85 foliations in the host rocks (mostly defined by the preferred orientation of biotite) have been measured. Note that due to the intense weathering and lack of well-exposed foliation planes, no mineral or stretching lineation (if present) were macroscopically detected within the entire intrusion nor in the country rock. No kinematic analysis was therefore possible.

In general, magmatic foliations are steep-dipping and follow the intrusion orientations. The overall pattern is fairly concentric in the km next to the rim, while towards the centre, orientations are more irregular and follow intrusive layers directions (Figure 7). In the country rock, main foliations are usually steep-dipping and display a nearly concentric pattern parallel to the intrusion borders. No sharp intrusive discordant contacts have been observed. This suggests that deformation occurred at relatively high temperatures, the intruded continental crust behaving quite ductile.

At the scale of the pluton, dikes are also generally steep-dipping and display a concentric organization (Figure 7). Nevertheless, their orientation at the outcrop scale is more irregular, many dikes being parallel to the main magmatic foliation but other cutting across the magmatic fabric, albeit at mostly low angles.

4.6. Magnetic field and gamma-ray data

The magnetic field and gamma-ray data were used prior and the after the fieldwork to prepare it and to enhance and confirm the interpretation of the field observations. The magnetic field (Figure 8a), with its regional long-wavelength component already removed with a 5000 m Butterworth Filter, replicates the observed nearly-ellipsoidal shape of the pluton. Its anomaly varies from −697 to 665 nT, in a predominant normal polarity for the Southern Hemisphere. The symmetric and mainly positive character of the Reduction to the Magnetic Pole (RTP) product confirmed the irrelevant to absent remanent magnetization in the source of the magnetic anomaly (Figure 8b). The adequate results from the RTP filtering allowed using further filtering as the Analytic Signal and Tilt Derivative over the RTP grid.

The Analytic Signal (Figure 8c) displayed the ellipsoidal contour of the pluton crosscut by two lineaments. The lineaments appeared in east–west direction and diverge to northwest and southeast as they invade the pluton area. Although well-characterized in the magnetic field map, these anomalies were not recognized in the field, suggesting that they did not propagate to the surface level, or were covered by a younger layer. A significant difference between the magnetic field data and the mapped lithology is the extension of the anomalies outwards the observed limits of the pluton in the surface. Such behaviour suggests that the pluton is actually larger in subsurface than it appears on the surface. Only the charnockite in the north part of the pluton and the norite spatially correlate with the observed anomalies (Figure 8c). The other lithologies can be magnetically too similar to permit their differentiation at 100 m terrain clearance (Table 1), whereas their contact with the metapelites is more than enough to generate considerable anomalies.

The use of the Tilt Derivative (Figure 8d) in association with the Analytic Signal suggested the presence of secondary lineaments accompanying the two main structures indicated solely by the Analytic Signal. These features may be linked to internal faulting or to the foliation. The fault observed invading the pluton from the west (Figure 2), did not cause a magnetic expression.

The gamma ray emissions divide the area in two, with a high K and eventual U peaks to the west and a predominance of Th to the east (Figure 8e). The area of the pluton has an enhancement of the three elements, but still marked by high K in its western portion – coherent with the presence of the charnockites. The porphyric pink alkali feldspar granite is followed by high counts of K, U and Th, especially in the north portion of the outcropped area of the pluton. High Th emissions continue to the east tapering to the area dominated by the drainage that runs towards

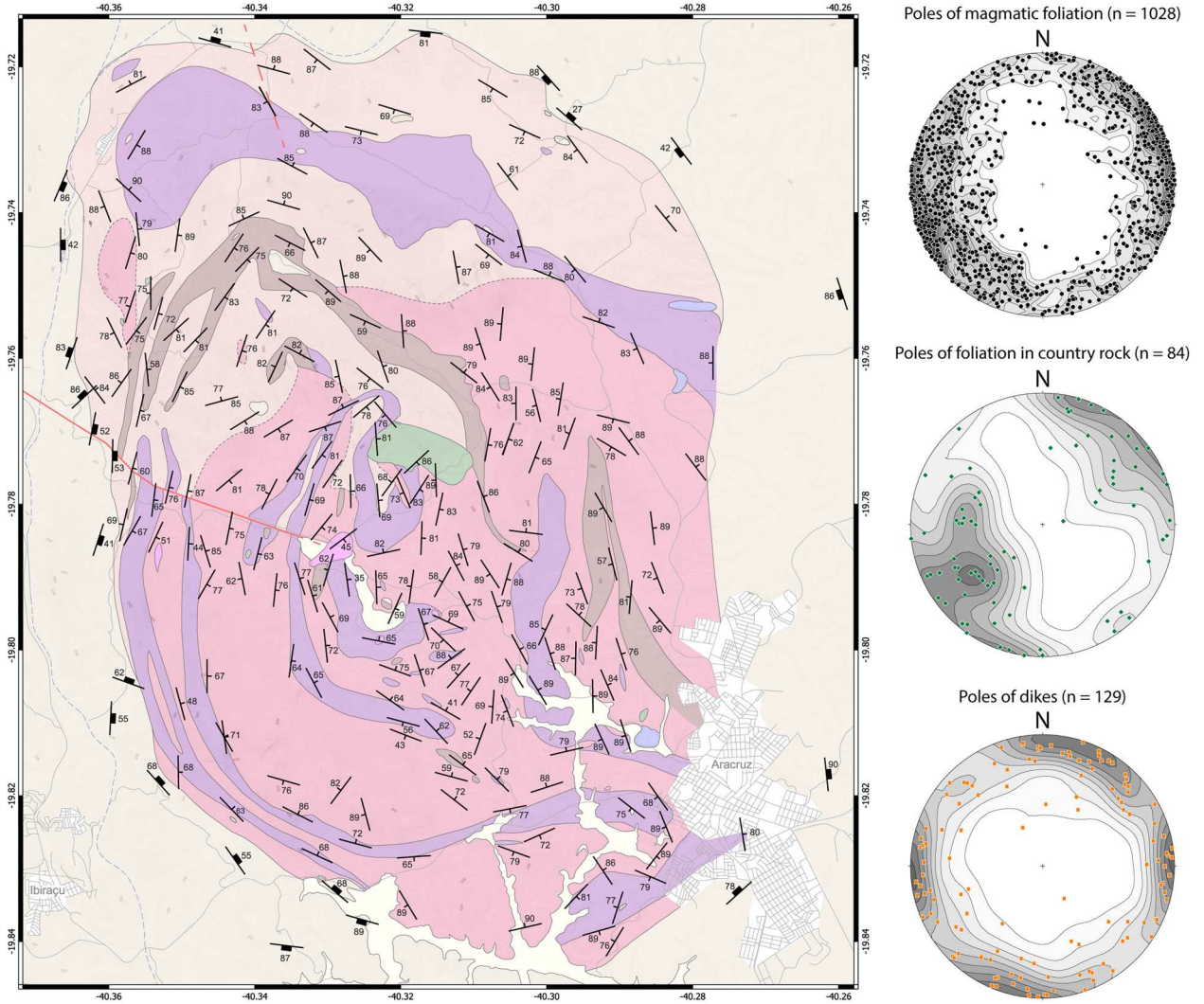

Figure 7. Map of the main foliation in both the Aracruz pluton and country rock displaying a selection of representative measurements, lithological units with same colours as in the main geological map (supplementary material), and stereographic projections of poles of magmatic foliations, dike orientation and main foliation in the country rock. Lower hemisphere equal area projections, N: number of measurements.

the same direction (Figure 8f). The fault at the west portion of the studied area coincides with a high Th lineament.

5. Discussion

5.1. Pluton architecture, assembly and sequence of intrusion

The detailed mapping of the Aracruz pluton coupled with magnetic field and Gamma-Ray data depicted its shape, extension and internal architecture, and revealed the relationship between the various intrusive units. The earliest and by far largest magma mass emplaced was the porphyric alkali feldspar granite, which was subsequently intruded by several tens to hundreds of meter thick often rim-parallel dike sheets of charnockite and quartz-diorite, which now form more or less continuous bands all across the pluton. The charnockite and quartz-diorite bands commonly align with the magmatic foliation of the porphyric alkali feldspar granite, suggesting that they mostly intruded into a crystal mush which still moved. Generally, quartz-diorite display a penetrative magmatic foliation defined by oriented amphibole and biotite crystals compared to the massive charnockites (Figure 4), which may indicate that the quartz-diorites are tendentially slightly older than the charnockites. Intrusive relations between the norite and surrounding granites (and charnockite and quartz-diorite) are unfortunately unclear, direct contacts are not observable. Nevertheless, the lack of flow structures in the massive norite and the nearly circular to slightly elliptical shapes of the norite bodies suggest that they were emplaced in a late-stage, as convection and magmatic deformation in the central part of the pluton ceased, although temperatures were still high enough to allow the crystallization of noritic bodies.

Through the southern part of the Araçuaí belt, several G5 plutons (e.g. Santa Angelica, Varzéa Alegre, Venda Nova, Mimoso do Sul plutons, e.g. De Campos et al., 2016) are typically inversely-zoned, displaying mafic cores surrounded by more evolved lithologies.

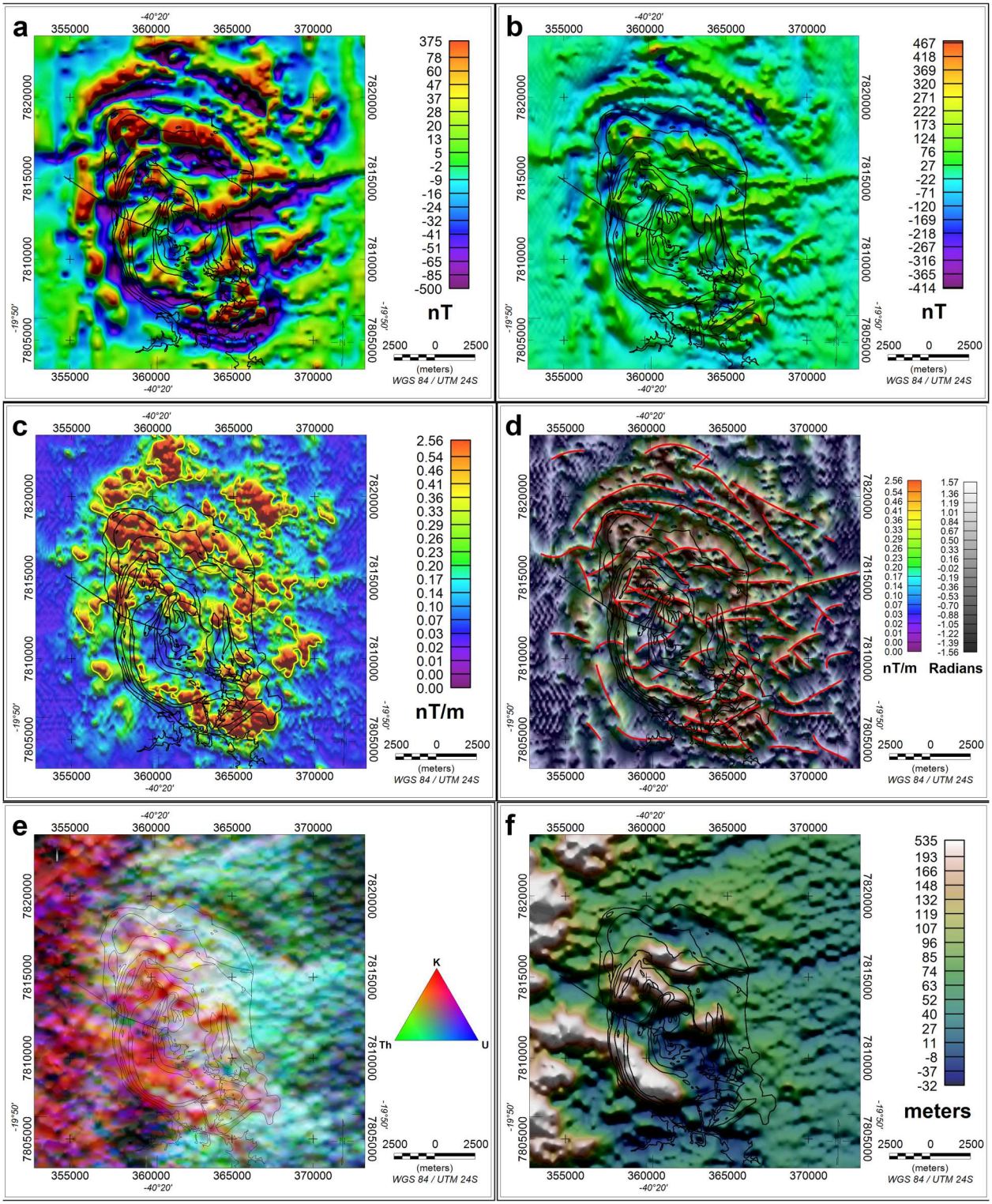

Figure 8. (a) Magnetic field map; (b) RTP map; (c) Analytic Signal including the contour of 0.32 nT/m, where the average maximum gradient occurs; (d) Composition of Analytic Signal and Tilt Derivative highlighting the magnetic lineaments in red lines; (e) Gamma-ray ternary image; and (f) Digital Terrain Model. All maps contain the contours of the lithologies and structures observed in the fieldwork.

Nevertheless, contrary to what is often reported, in the Aracruz pluton a regularly developed chemically concentric form with mafics in the centre, systematically followed by intermediate compositions and finishing with granites towards the border does not exist. In contrast, the relations between rock types is geometrically more complex and testifies for at least three distinct magma types intruding separately into the (porphyric) granitic crystal mush. The limited mixing or mingling in the homogeneous granite - compared to the heterogenous granite - is best explained by a distinctly higher viscosity of the former. In the southern and central part, the intrusion of the charnockite and quartz-diorite occurred when the porphyric alkali

feldspar granite was already quite viscous and convection therefore moderate, such that the disruption of the intermediate melts was limited. Only occasional enclave swarms, still oriented in the magmatic foliation, testify for dissolution of intermediate injections into the mush of the homogeneous granite. Instead, the northern heterogeneous granite displays a different picture. Typically, outcrops have 5-40% darker, finer grained intermediate charnockite to quartz-diorite, always oriented in the main foliation, individual bodies or enclaves are mostly just 10–100 cm wide and 0.5-10 m in length. The intermediate magmas are completely disrupted, and chemical dissolution in the granite is documented by many 'schlieren' of mafic minerals in the granite. The amount of fine-grained intrusives in the coarse-grained porphyric heterogeneous alkali feldspar granite is also heterogeneous from outcrop to outcrop, an overall pattern not recognizable. It is hence evident, that the heterogeneous granite was less viscous than the homogeneous one and still had some rigor of convecting dynamics leading to ample disruption of the intermediate intrusives. Whether the homogeneous and heterogeneous granite are two distinct magma batches or the same magma batch in two different physical states cannot be unraveled by the mapping and microscopic observations.

5.2. Emplacement mechanism

A the scale of the pluton, the lack of sharp intrusive discordant contacts to the country rock and the nearly complete absence of xenoliths within the intrusives preclude stoping as main emplacement mechanism (Glazner & Bartley, 2006 and references therein). The nearly concentric orientations of the main foliations in the country rock sub-parallel to the contacts with the Aracruz pluton and their deviations from the regional structural NNE-SSW oriented trend suggest ballooning, the in-situ, symmetrical, magma body growth by radial expansion (Paterson & Vernon, 1995), or diapirism, the upward movement of magma masses through the crust (Van den Eeckhout et al., 1986), as plausible modes of emplacement (e.g., discussion in Molyneux & Hutton, 2000), in any case indicating that the pluton emplaced as the crust was warm enough to deform in a ductile regime. In general, both ballooning and diapirism are expected to account also for subcircular pluton shapes in map view, steep-dipping, nearly concentric internal magmatic fabric arrangement and chemical zoning, all features reported from the Aracruz pluton. The complex internal architecture of the pluton outlined by numerous charnockite and quartz-diorite bands intruding the granites mostly in a dynamic environment (see above) and the lack of a regularly concentric chemical zoning suggest that the Aracruz pluton was emplaced rather by diapirism than by ballooning, similar to other post-orogen plutons in the central and southern part of the Araçuaí belt (e.g. Santa Angelica pluton, De Campos et al., 2004; Souza Junior et al., 2021; Temporim et al., 2020), where buoyancy-driven diapirism followed by a reverse diapiric mechanism after cooling is invoked as emplacement mechanism (Bayer et al., 1987; Souza Junior et al., 2021). Instead, in the northern part of the orogen, which exposes 1–2 kbar shallower and therefore cooler crustal levels (Pedrosa-Soares et al., 2011), the host crust did not allow further magma ascent but caused the lateral spread of magma flow and the consequent formation of flat-floored large granitic and charnockitic plutons without mafics (e.g. Medina batholith, Serrano et al., 2018). To establish the exact mechanism of emplacement for the Aracruz pluton a detailed investigation of microstructures and magnetic fabric within the pluton together with an accurate kinematic analysis in the country rock all around the intrusion are required, a meticulous study of the lineation (if existing) is necessary.

5.3. Origin(s) of magmas

Many post-collisional G5 plutons through the Araçuaí belt display a bimodal geochemical and isotopic composition (e.g. Pedrosa-Soares et al., 2011), which is interpreted to result from the partial melting of two different sources, an enriched mantle and the lower crust (De Campos et al., 2004). Following this interpretation, large silicic G5 batholiths arose from the mixing of mantle-derived and crustal melts. In the Aracruz pluton, the norite, charnockite and quartz-diorite clearly originated in the mantle, whereas the lack of Al-rich phases, such as muscovite, garnet and cordierite in the granites suggests that the latter did not result from pure intra-crustal melting but rather by differentiation of mantle-derived melts ± interaction with the host crust. As shown by many studies (e.g. Ulmer et al., 2018), the complete rock suite from gabbronorites to granites can be produced by the progressive fractionation of olivine, pyroxenes, amphibole, plagioclase, oxides ± apatite in a closed-system, whereas the interaction of gabbroic melts with pelitic material is expected to stabilize orthopyroxene at the expense of clinopyroxene producing norites (Beard et al., 2017), interaction which is especially plausible in the lower crust during an early stage of the magmatic evolution as the assimilation of crustal material is thermally favored. To retrieve if the different magma batches (porphyric granite, quartz-diorite, charnockite, norite) simply reflect distinct degrees of differentiation of the same parental melt in a closed-system and likely shared a similar ± metasomatized mantle source, or if the magmatic system was affected at different extents by crustal contamination during its evolutions, geochemical and isotopic analyses are required.

Irrespective of the amount of interaction with the host crust, the relative sequence of intrusion porphyric granite – quartz-diorite – charnockite – norite inferred by field observations cannot be achieved through differentiation of a single batch of magma by fractional crystallization nor due to the interaction of granitic magmas with crustal material, but rather indicates that the Aracruz pluton was progressively assembled through the intrusion of several mantle-derived batches of intermediate to mafic magmas into a compositionally more evolved granitic mush.

6. Conclusions

Field relations show that the Aracruz pluton was constructed by the progressively intrusion of four major magma types emplaced by buoyancy-driven diapirism. The first magma was emplaced as a porphyric alkali feldspar granite, which was subsequently intruded by 100 m to km wide dike sheets of charnockite and quartz-diorite. These bands were deformed together with the host granites when all magmas were not fully solidified but still in a mushy stage and partly convecting, forming the now observable complex band arrangement. The abundant occurrence of charnockitic and quartz-dioritic enclaves and schlieren in the heterogeneous granite in the north compared to the more homogeneous central and southern granite indicate a distinct rheology and dynamics of the host granite during the emplacement of charnockites and quartz-diorites, which in the north intruded when the granite was less viscous and likely undergoing stronger convection than in the south. Charnockites and quartz-diorites were deformed and often dismembered, and are now present as dikelets and enclaves aligned within the magmatic flow foliation of the host granite. In the central and southern part of the pluton, the granite is petrologically identical to the northern granite and also has a clear magmatic flow foliation best visible in the field by the alignment of the porphyric alkali feldspars but remained homogeneous. As the last magma pulse, a central noritic body that does not show any internal deformation was intruded. In the map, this norite crosscuts all previous intrusives, yet contacts could not be observed. Finally, a few granitic dikes crosscutting the magmatic foliation were emplaced, in total, only a few of these were observed in the entire pluton. The intrusion of large magma volumes of mafic to intermediate composition testifies for an intense mantle activity during the post-orogenic stage of the Araçuaí orogen in response to lithospheric thinning following gravitational collapse, and shows that new continental crust can be produced during the final stages of a Wylson cycle. Apart from two larger regional faults running into and terminating in the pluton, there is a striking absence of post-magmatic deformation or alteration, which ultimately renders these post-orogenic Cambrian plutons ideal for ornamental stones.

7. An outcrop guide for visits to the aracruz pluton

In the following, we shortly describe a set of outcrops optimized for accessibility, which typify best the geology of the Aracruz pluton. They are given in a separate map in supplementary material. Outcrop coordinates and coordinates where to best stop the vehicle are provided below.

(A) Norite (Point A1, outcrop coordinates: 040° 18’49.247181’’W/19°46’28.583905’’S; parking facilities: 040°18’48.083701’’W/19°46’29.710153’’S; Point A2, outcrop coordinates: 040° 19’04.006238’’W/ 19°46’19.896571’’S; parking facilities: 040°18’48.083701’’W/19°46’29.710153’’S): The norite is to be visited in one of the two quarries (Gransal Granitos Aracruz – Point A1, and Imetame Monte Serrat – Point A2), which both express the same features. An appointment is recommended. The most impressive feature is the massiveness and homogeneity over 2 km. Blocks from the quarries can also be found on the main road leading from the NE to those (Estrada do Mont Serrat).

(B) Charnockite (outcrop coordinates: 040° 19’27.320624’’W/19°46’58.021362’’S; parking facilities: 040°19’29.275968’’W/19°46’56.638529’’S): Typical massive charnockite and its intruding porphyric granitic dikes can be observed ca 100 meters SW from the entrance of Sitio Flor da Vida, directly southern of the main road.

(C) Quartz-diorite (Point C1, outcrop coordinates: 040°18’31.969325’’W/19°46’16.583717’’S; parking facilities: 040°18’33.779338’’W/19° 46’18.757055’’S; Point C2, outcrop coordinates: 040°18’19.375196’’W/ 19°45’47.887733’’S; parking facilities: 040°18’17.776571’’W/19° 45’47.742403’’S): a typical outcrop of quartz-diorite is just east of the main road leading to the quarries, a few hundred meter NE of the quarries (Point C1), note the magmatic foliation, the parallelized dikes and the cross-cutting conjugate dikes. A small outcrop (Point C2) is also 400 m west of the sawed road cut described below.

(D) Homogeneous porphyric grey alkali feldspar granite (Point D1, outcrop coordinates: 040° 17’59.903015’’W/19°49’06.295628’’S; parking facilities: 040°17’59.241105’’W/19°49’08.515207’’S; Point D2, outcrop coordinates: 040° 18’11.207014’’W/19°49’43.291252’’S; parking

facilities: 040°18’01.520137’’W/19°49’24.519956’’S): This granite can be well observed on any of the larger cupola shaped outcrops in the southern two thirds of the pluton. We could recommend a small hill next to the Sitio Santa Joana (Point D1), about 400 m further west from the quarry Padramix Aracruz. On the southern side of the Aracruz-Ibiraçu road, you can enter in a 2 km long walk through the homogenous granite on a gated (and closed) southbound road (Point D2). Ask the owner of Cadablio Mármores e Granitos for permission.

(E) Heterogeneous porphyric grey alkali feldspar granite (outcrop coordinates: 040°20’59.038888’’W/ 19°46’41.051933’’S; parking facilities: 040°20’57.806229’’W/19°46’39.977815’’S): The contrast between the homogenous and heterogeneous porphyric grey alkali feldspar granite types can be best visited at their boundary in the valley formed by the João Neiva fault. The location is a few km into the pluton, follow the road on the northern side of the valley. Coming from the west, you will see a quadratic abandoned house and drive across a series of typical heterogeneous porphyric granite outcrops. A few hundred meters further, cupola shaped hills with homogeneous porphyric granite begin.

(F) Transition from granite to charnockite (outcrop coordinates: 040°17’21.761930’’W/ 19°48’56.882235’’S; parking facilities: 040°17’40.667986’’W/19°49’13.600421’’S): the southern quarry (Pedramix Aracruz) typifies the homogenous porphyric alkali feldspar granite in its northern inactive part while the southern active walls do show the transition from granite to charnockite with the typically heterogeneous boundary zone. In this zone, a panoply of small interacting magma batches can be identified as stocks, dikes and schlieren. This quarry produces gravel but not ornamental stones the entrance locates about 1 km from the rim of Aracruz city on the road towards Iribaçu (ES-257). An appointment is recommended.

(G) Porphyric pink alkali feldspar granite (outcrop coordinates: 040°19’38.958660’’W/19°47’08.196194’’S; parking facilities: 040°19’37.811217’’W/19°47’09.498215’’S): The porphyric pink alkali feldspar granite is well observable just adjacent to a crossing of the road leading southwards from the norite quarries to the one crosscutting the Aracruz pluton east–west. Fresh handspecimen can be recovered in a small dig out, there, the redish alkali feldspar but white to grey to black matrix demonstrates that the red colour is not a weathering feature.

(H) Aplite dikes (outcrop coordinates: 040°18’15.777959’’W/19°45’41.055922’’S; parking facilities: 040°18’25.088300’’W/19°45’42.919774’’S): Rare, fine-grained, discordant granitic late-stage dikes occur in homogenous granite north of the road to the main quarry.

(I) Crustal assimilation in action (outcrop coordinates: 040°18’00.394493’’W/19°45’52.350507’’S; parking facilities: 040°18’02.873684’’W/19°45’53.483087’’S): Along the road Estrada do Mont Serrat, there is a sawed ca. 2 m high face that has a small amount of country rock dispersed in otherwise homogeneous granite. Here some assimilation and the formation of garnet can be observed (otherwise we did not find any garnet in the porphyric granite).

(J) Tension gaps (outcrop coordinates: 040°20’29.162358’’W/19°44’26.158928’’S; parking facilities: 040°20’28.608052’’W/19°44’25.624687’’S): The best example of tension gaps into which quartz, alkali feldspar and biotite crystallized occurs on several boulders within a coffee plantation 10 meters to the south of a cattel rost + gate on the road that leads from the Igreja de São Caetano to the NW.

(K) Nova Venécia complex (outcrop coordinates: 040°19’54.043224’’W/19°43’02.541433’’S; parking facilities: 040°19’59.357417’’W/19°43’07.093768’’S): upper amphibolite facies migmatitic metasediments directly adjacent to the pluton can be best observed in the ca. 15 m deep train track cut in the NW, just east of the train bridge across the main BR101 highway. Access is through a dirt road branching of BR101, 100 m S of the bridge. A short walk through some bushes is required, yet this 500 m long perfectly outcropping sections shows all characteristics of the Nova Venécia complex.

(L) Contact Aracruz pluton / country rock (Point L1, outcrop coordinates: 040°19’53.584698’’W/ 19°43’04.935171’’S; parking facilities: 040°19’54.043224’’W/19°43’02.541433’’S; Point L2, outcrop coordinates: 040°18’01.530470’’W/19°43’19.951294’’S; parking facilities: 040°17’44.807221’’W/ 19°43’28.736172’’S): A truly outcropping contact of the pluton with the Nova Venécia country rocks may only be observed in two spots. One is the southern shoulder of the train track cut (Point L1), where one can observe a much finer grain and more porphyroclastic appearance of the granite, deformation directly at the contact being much more intense. The other spot (Point L2) is a hill side, in the NE of the pluton, where a steep continuous

outcrop reaching hundred meter into each lithology can be investigated.

(M) Banded orthogneiss (outcrop coordinates: 040° 15'31.134103''W/19°45'00.793986''S; parking facilities: 040°15'30.955396''W/19°44'59.702930''S): fresh representative outcrops of banded orthogneisses are exposed in a river bed directly east of a small bridge on a dirty road.

(N) Mesozoic fine-grained basaltic dike (outcrop coordinates: 040°19'44.000339''W/19°49'26.089790''S; parking facilities: 040°19'41.902879''W/19°49'48.273019''S): the only mapped Mesozoic basaltic dyke occurs in the Parque Natural Municipal do Aricanga. You can leave the car at the park entrancy and follow the path along the Trilhada Gruta path through the forest.

(O) Ferruginized sandstones (outcrop coordinates: 040°17'13.845384''W/19°48'41.082181''S; parking facilities: 040°17'16.855193''W/19°48'41.841600''S): The Miocene sediments of the Barreiras formation and their mineralization can be best observed in the hill side just west of the northernmost deeply incised valley of NW Aracruz. Walk up the steep west face of the hill.

Software

All collected data have been stored in a digital georeferenced database and a digital geological map have been designed using the 3.30 version of the free and open source QGIS software (QGIS.org, 2023, QGIS Geographic Information System, Open Source Geospatial Foundation Project, http://qgis.org) and Adobe Illustrator 2024.

Acknowledgements

We thank the quarry and land owners for their generous permissions to work on their property. We are thankful to Dr. Kryštof Verner, Dr. Jose Francisco Molina and Dr. Thomas Pingel for their constructive reviews of the manuscript and to Dr. Claudio Riccomini for his editorial work.

Disclosure statement

No potential conflict of interest was reported by the author(s).

Funding

This work was made possible through the support of the Burri-Grubenmann donation to the Institute of Mineralogy and Petrology, ETH Zurich.

Data availability statement

The authors attest that the data presented in this study are available within the paper or as supplementary material.

References

Alkmim, F. F., Marshak, S., Pedrosa-Soares, A. C., Peres, G. G., Cruz, S. C. P., & Whittinton, A. (2006). Kinematic evolution of the Araçuaí-West Congo Orogen in Brazil and Africa: Nutcracker tectonics during the neoproterozoic assembly of Gondwana. *Precambrian Research*, *149* (1-2), 43–64. https://doi.org/10.1016/j.precamres.2006.06.007

Bayer, P., Schmidt-Thomé, R., Weber-Diefenbach, K., & Horn, H. A. (1987). Complex concentric granitoid intrusions in the coastal mobile belt, Espírito Santo, Brazil: the Santa Angélica Pluton – and example. *Geologische Rundschau*, *76*(2), 357–371. https://doi.org/10.1007/BF01821080

Beard, J. S., Fedele, L., & Bodnar, R. J. (2017). A quartz-bearing norite formed by the Bowen reaction at a diorite-pelite contact. *Geology*, *45*(10), 883–886. https://doi.org/10.1130/G39264.1

Bento, T. B., de Newman, D., & dos Santos, J. (2022). Aspectos químico-mineralógicos das escapolitas de Aracruz e Nova Venécia – ES. *Geociências*, *41*(1), 75–87. https://doi.org/10.5016/geociencias.v41i1.16414

Bley de Britos Neves, B., Fuck, R. A., & Pimentel, M. M. (2014). The Brasiliano collage in South America: A review. *Brazilian Journal of Geology*, *44*(3), 493–518. https://doi.org/10.5327/Z2317-4889201400030010

Bonin, B. (2004). Do coeval mafic and felsic magmas in post-collisional to within-plate regimes necessarily imply two contrasting, mantle and crustal, sources? A review. *Lithos*, *78*(1-2), 1–24. https://doi.org/10.1016/j.lithos.2004.04.042

Cavalcante, C., Fossen, H., de Almeida, R. P., Hollanda, M. H. B., & Egydio-Silva, M. (2019). Reviewing the puzzling intracontinental termination of the Araçuaí-West Congo orogenic belt and its implications for orogenic development. *Precambrian Research*, *322*, 85–98. https://doi.org/10.1016/j.precamres.2018.12.025

De Campos, C. P., De Medeiros, S. R., Mendes, J. C., Pedrosa-Soares, A. C., Dussin, I., Ludka, I. P., & Dantas, E. L. (2016). Cambro-Ordovician magmatism in the Araçuaí Belt (SE Brazil): snapshots from a post-collisional event. *Journal of South American Earth Sciences*, *68*, 248–268. https://doi.org/10.1016/j.jsames.2015.11.016

De Campos, C. P., Mendes, J. C., Ludka, I. P., Medeiros, S. R., Moura, J. C., & Wallfass, C. (2004). A review of the Brasiliano magmatism in southern Espírito Santo, Brazil, with emphasis on post-collisional magmatism. *Journal of the Virtual Explorer*, *17*. https://doi.org/10.3809/jvirtex.2004.00106

Figueiredo, M. C. H., & Campos Neto, M. C. (1993). Geochemistry of the Rio Doce magmatic arc, southeastern Brazil. *Anais da Academia Brasileira de Ciências*, *65*, 63–81.

Fortes, P., Bastos, A. C., Lana, C. E., Althoff, F. J., Espinoza, J. A., & Campos, R. (2014). *Carta geológica: folha SE-24-Y-D-IV Aracruz*. Repositório Institucional de Geociências CPRM. https://rigeo.sgb.gov.br/handle/doc/18319

Glazner, A. F., & Bartley, J. M. (2006). Is stoping a volumetrically significant pluton emplacement process? *GSA Bulletin*, *118*(9-10), 1185–1195. https://doi.org/10.1130/B25738.1

Goméz-Frutos, D., Castro, A., & Gutiérrez-Alonso, G. (2023). Post-collisional batholiths do contribute to continental growth. *Earth and Planetary Sciences Letters*, *603*, 117978. https://doi.org/10.1016/j.epsl.2022.117978

Gonçalves, L., Alkmim, F. F., Pedrosa-Soares, A. C., Dussin, I. A., Valeriano, C. M., Lana, C., & Tedeschi, M. (2016). Granites of the intracontinental termination of a magmatic arc: An example from the Ediacaran Araçuaí Orogen, Southeastern Brazil. *Gondwana Research*, *36*, 439–458. https://doi.org/10.1016/j.gr.2015.07.015

Gradim, C., Roncato, J., Pedrosa-Soares, A. C., Cordani, U. G., Dussin, I., Alkmim, F. F., Queiroga, G., Jacobsohn, T., Silva, L. C., & Babinski, M. (2014). The hot back-arc zone of the Araçuaí orogen, Eastern Brazil: From sedimentation to granite generation. *Brazilian Journal of Geology*, *44*(1), 155–180. https://doi.org/10.5327/Z2317-4889201400010012

MacLeod, I. N., Jones, K., & Dai, T. F. (1993). 3-D analytic signal in the interpretation of total magnetic field data at low magnetic latitudes. *Exploration Geophysics*, *24*(4), 679. https://doi.org/10.1071/eg993679

Miller, H. G., & Singh, V. (1994). Potential field tilt—a new concept for location of potential field sources. *Journal of Applied Geophysics*, *32*(2-3), 213–217. https://doi.org/10.1016/0926-9851(94)90022-1

Molyneux, S. J., & Hutton, D. H. W. (2000). Evidence for significant granite space creation by the ballooning mechanism: The example of the Ardara pluton, Ireland. *GSA Bulletin*, *112*(10), 1543–1558. https://doi.org/10.1130/0016-7606(2000)112<1543:EFSGSC>2.0.CO;2

Monteiro, H. S., Vasconcelos, P. M., Farley, K. A., Mello, C. L., & Conceiçao, F. T. (2022). Long-term vegetation-induced goethite and hematite dissolution-reprecipitation along the Brazilian Atlantic margin. *Palaeogeography, Palaeoclimatology, Palaeoecology*, *601*, 111137. https://doi.org/10.1016/j.palaeo.2022.111137

Muir, R. J. (2015). Digital field mapping – making the change from paper to touchscreen technology. *Geology Today*, *31 (6)*(6), 232–236. https://doi.org/10.1111/gto.12120

Nalini, H. A., Bilal, E., & Correia-Neves, J. M. (2000). Syncollisional peraluminous magmatism in the Rio Doce region: Mineralogy, geochemistry and isotopic data of the Urucum suite (eastern Minas Gerais State, Brazil). *Revista Brasileira de Geociências*, *30*(1), 120–125. https://doi.org/10.25249/0375-7536.2000301120125

Neves, B. B. B., & Cordani, U. G. (1991). Tectonic evolution of South America during the late Proterozoic. *Precambrian Research*, *53*(1-2), 23–40. https://doi.org/10.1016/0301-9268(91)90004-T

Onken, C. T., Eberhard-Schmid, J., Hauser, L., Marioni, S., Galli, A., Janasi, V. A., & Schmidt, M. W. (2024). Timing and origin of the post-collisional Venda Nova and Varzéa Alegre Plutons from the Araçuaí belt, Espírito Santo, Brazil. *Lithos*, *482–483*, 107677. https://doi.org/10.1016/j.lithos.2024.107677

Paterson, S. R., & Vernon, R. H. (1995). Bursting the bubble of ballooning plutons: A return to nested diapirs emplaced by multiple processes. *GSA Bulletin*, *107*(11), 1356–1380. https://doi.org/10.1130/0016-7606(1995)107<1356:BTBOBP>2.3.CO;2

Pedrosa-Soares, A. C., De Campos, C., Noce, C. M., Silva, L. C., Novo, T., Roncato, J., Medeiros, S., Castañeda, C., Queiroga, G., Dantas, E., Dussin, I., & Alkmim, F. F. (2011). Late Neoproterozoic-Cambrian granitic magmatism in the Araçuaí orogen (Brazil), the Eastern Brazilian Pegmatite Province and related mineral resources. *Geological Society of London Special Publications*, *350*(1), 25–51. https://doi.org/10.1144/SP350.3

Pedrosa-Soares, A. C., Noce, C. M., Wiedemann, C. M., & Pinto, C. P. (2001). The Araçuaí-West-Congo Orogen in Brazil: An overview of a confined orogen formed during Gondwanaland assembly. *Precambrian Research*, *110*(1-4), 307–323. https://doi.org/10.1016/S0301-9268(01)00174-7

Richter, F., Lana, C., Stevens, G., Buick, I., Pedrosa-Soares, A. C., Alkmim, F. F., & Cutts, K. (2016). Sedimentation, metamorphism and granite generation in a back-arc region: Records from the Ediacaran Nova Venécia Complex (Araçuaí Orogen, Southeastern Brazil). *Precambrian Research*, *272*, 78–100. https://doi.org/10.1016/j.precamres.2015.10.012

Santiago, R., de Andrade Caxito, F., Neves, M. A., Dantas, E. L., de Medeiros Júnior, E. B., & Nascimento Queiroga, G. (2020). Two generations of mafic dyke swarms in the Southeastern Brazilian coast: reactivation of structural lineaments during the gravitational collapse of the Aracuai-Ribeira Orogen (500 Ma) and West Gondwana breakup (140 Ma). *Precambrian Research*, *340*, 105344. https://doi.org/10.1016/j.precamres.2019.105344

Serrano, P., Pedrosa-Soares, A. C., Medeiros-Junior, E., Fonte-Boa, T., Araujo, C., Dussin, I., Queiroga, G., & Lana, C. (2018). A-type Medina batholith and post-collisional anatexis in the Araçuaí orogen (SE Brazil). *Lithos*, *320-321*, 515–536. https://doi.org/10.1016/j.lithos.2018.09.009

Sluitner, Z., & Weber-Diefenbach, K. (1989). Geochemistry of charnoenderbitic granulites and associated amphibolitic gneisses in the Coast Region of Espírito Santo, Brazil. *Zentralblatt für Geologie und Paläontologie Teil I*, *Heft 5/6*, 917–931.

Souza Junior, G. F., Trindade, R. I. F., Temporim, F. A., Bellon, U. D., Gouvêa, L. P., Soares, C. C., Amaral, C. A. D., & Louro, V. (2021). Imaging the roots of a post-collisional pluton: Implications for the voluminous Cambrian magmatism in the Araçuaí orogen (Brazil). *Tectonophysics*, *821*, 229146. https://doi.org/10.1016/j.tecto.2021.229146

Temporim, F. A., Trindade, R. I. F., Tohver, E., Soares, C. C., Gouvêa, L. P., Egydio-Silva, M., Amaral, C. A. D., & Souza Junior, G. F. (2020). Magnetic Fabric and Geochronology of a Cambrian "Isotropic" Pluton in the Neoproterozoic Araçuaí Orogen. Tectonics 39. https://doi.org/10.1029/2019TC005877.

Trompette, R. (1997). Neoproterozoic (ca. 600 Ma) aggregation of Western Gondwana: A tentative scenario. *Precambrian Research*, *82*(1-2), 101–112. https://doi.org/10.1016/S0301-9268(96)00045-9

Ulmer, P., Kägi, R., & Müntener, O. (2018). Experimentally derived intermediate to silica-rich Arc magmas by fractional and equilibrium crystallization at 1.0 GPa: An evaluation of phase relationships, compositions, liquid lines of descent and oxygen fugacity. *Journal of Petrology*, *59*(1), 11–58. https://doi.org/10.1093/petrology/egy017

Van den Eeckhout, B., Grocott, J., & Vissers, R. (1986). On the role of diapirism in the segregation, ascent and final emplacement of granitoid magmas—discussion. *Tectonophysics*, *127*(1-2), 161–169. https://doi.org/10.1016/0040-1951(86)90086-7

Vauchez, A., Egydio-Silva, M., Babinski, M., Tommasi, M., Uhlein, A., & Liu, D. (2007). Deformation of a pervasively molten middle crust: Insights from the Neoproterozoic Ribeira-Arc, Araçuaí orogen (SE Brazil). *Terra Nova*, *19*(4), 278–286. https://doi.org/10.1111/j.1365-3121.2007.00747.x

Vieira, R. A. B., Mendes, M. P., Vieira, P. E., Costa, L. A. R., Tagliari, C. V., Barcelar, L. A. P., & Feijó, F. J. (1994). Bacias do Espírito Santo e Mucurí. *Boletim de Geosciências Petrobras*, *8*(1), 191–202.

Vieira, V. S., Silva, M. A., Corrêa, T. R., & Lopes, N. H. (2018). *Mapa geológico do estado do Espírito Santo*. Repositório Institucional de Geociências CPRM. https://rigeo.sgb.gov.br/handle/doc/15564

Wiedemann, C. M., De Medeiros, S. R., Ludka, I. P., Mendes, J. C., & Costa-de-Moura, J. (2002). Architecture of late orogenic plutons in the Araçuaí-Ribeira Fold Belt, Southeast Brazil. *Gondwana Research*, *5*(2), 381–399. https://doi.org/10.1016/S1342-937X(05)70730-9

Wisniowski, L., Pedrosa-Soares, A. C., Medeiros-Junior, E., Belém, J., Dussin, I., & Queiroga, G. (2021). Ultra-high temperature, mid-crustal level, contact metamorphism imprinted on granulite facies paragneisses by a norite intrusion (São Gabriel da Baunilha, Araçuaí orogen, southeast Brazil). *Journal of Metamorphic Geology*, *39*(7), 867–895. https://doi.org/10.1111/jmg.12594